Description and crystal structure of turtmannite, a new mineral with a 68 Å period related to mcgovernite

JOËL BRUGGER,[1],* THOMAS ARMBRUSTER,[2] NICOLAS MEISSER,[3] CLIVIA HEJNY,[2] AND BERNARD GROBETY[4]

[1]VIEPS, Department of Earth Sciences, P.O. Box 28E, Monash University, VIC-3800, Australia
[2]Laboratorium für Chemische und Mineralogische Kristallographie, Universität Bern, Freiestrasse 3, CH-3012 Bern, Switzerland
[3]Musée Géologique Cantonal & Laboratoire des Rayons-X, Institut de Minéralogie, UNIL-BFSH2, CH-1015 Lausanne-Dorigny, Switzerland
[4]Institut de Minéralogie et Pétrographie, Université de Fribourg, Pérolles, CH-1700 Fribourg, Switzerland

ABSTRACT

Jacobsite-rich Fe-Mn ores of probable Dogger age fill paleokarst pockets in the Triassic marbles of the Barrhorn Unit under Pipjigletscher in the Turtmanntal, Valais, Switzerland. These ores and embedding rocks underwent Tertiary metamorphism under upper greenschist facies conditions. Some of these jacobsite ores contain minor amounts of a yellow micaceous mineral, which appears to be a new Mn-Mg silicate-vanadate-arsenate that was named "turtmannite" with respect to the type locality. Turtmannite flakes up to 200 μm in length occur parallel to the main schistosity, or fill thin discordant veinlets. Turtmannite is rhombohedral $R\bar{3}c$, with $a_H = 8.259(2)$ and $c_H = 204.3(3)$ Å in the hexagonal setting. The corresponding primitive rhombohedral cell has $a_R = 68.31$ and $\alpha_R = 6.92°$. HRTEM images indicate that turtmannite is perfectly ordered along **c**.

The structure of turtmannite has been solved to a final $R1$ of 12.4% on a Siemens Smart CCD diffractometer with Mo$K\alpha$ X-radiation, and a detector to sample distance extended to 12 cm. The structure consists of 84 oxygen layers stacked along **c**, with twelve close-packed layers followed by two non-close-packed layers. This sequence is repeated six times. The structure contains eight symmetrically distinct cation layers. Three different occupational variants have been recognized leading to the following hypothetical end-member formulae and approximate abundances:

I	$^{[IV]}Mn_{1.5}\,^{[IV]}Mg_3\,^{[VI]}(Mn,Mg)_{21}[(V,As)O_4]_3[SiO_4]_3O_5(OH)_{20}$,	50%
II	$^{[IV]}Mn_{1.5}\,^{[VI]}(Mn,Mg)_{21}[(V,As)O_4]_3[SiO_4]_3[AsO_3](OH)_{21}$	33%
III	$^{[IV]}Mn_{1.5}\,^{[VI]}(Mn,Mg)_{21}[(V,As)O_4]_3[SiO_4]_2[SiO_3OH](OH)_{25}$	16%

The simplified chemical formula for turtmannite can be written as:

$$(Mn,Mg)_{22.5}Mg_{3-3x}[(V,As)O_4]_3[SiO_4]_3[AsO_3]_xO_{5-5x}(OH)_{20+x}.$$

The unit cell of turtmannite is similar to those of mcgovernite, a Mn-Mg-Zn arsenate from Sterling Hill, New Jersey, and an unnamed "mcgovernite-like" Mn-Mg arsenate from the Kombat Mine, Namibia. The crystal structure of turtmannite is close to the model predicted for mcgovernite by Moore and Araki (1978).

INTRODUCTION

The mineralogical study of manganoan ores filling paleokarst pockets that outcrop under the suspended Pipjigletscher (glacier) in the Triassic marbles of the Barrhorn Unit in the Central Alps, Switzerland, has revealed the presence of several As- and V-rich phases. In this communication, we report the description and crystal structure of one of these minerals, which has been accepted by the International Miner-alogical Association as the new mineral "turtmannite." The holotype (MGL53593) and cotype (MGL58732) are deposited at the "Musée Cantonal de Géologie," Lausanne, Switzerland. The mineral is named after the Turtmann Valley that hosts the type locality and also has a rich geological background and mining history. Thrust sheet tectonic was discovered in the Turtmann valley (Gerlach 1869; Argand 1911), and several high altitude 19th century Ni-Co mines are located in the valley (e.g., Plantorin at 3031 m altitude; Schafer 1994).

THE MANGANOAN PALEOKARST LENSES AT PIPJIGLETSCHER

The Turtmanntal, a tributary to the Rhone Valley in Canton Wallis, Central Alps, Switzerland, is located in the Middle

* Present Address: South Australian Museum and Adelaide University, North Terrace, 5000 Adelaide, Australia. E-mail: Brugger.Joel@saugov.sa.gov.au

Penninic (Briançonnais Domain) Siviez-Mischabel super-nappe (Escher et al. 1987). In the upper part of the valley, the pre-Mesozoic crystalline rocks of the "Ensemble de l'Ergischhorn" are overlain by the sediments of the Barrhorn Series. The Barrhorn Series is one of the rare Mesozoic covers of the Briançonnais domain that is still bound to its original basement (Sartori 1990). Paleokarst pockets occur within the Triassic marbles at the basis of the series (Sartori 1990), and are filled with various sediments of probable Dogger age, with compositions ranging from aluminous (bauxite) to ferruginous (hematite and/or magnetite-rich). At one locality, in the cliff forming the right rim of the ice fall of the Pipjigletscher (coordinates on the Swiss National Reference System: 112.450/622.550; 3030 m), a unique type of manganoan karst filling was discovered by Sartori (1990). The black ores occur in a line of compressed pockets, measuring up to 1 m by 0.3 m. These paleokarst pockets are embedded in grey dolomitic marbles of the "Couches à C. Goldfussi" (Ladinian). The paleokarst fillings and the embedding rocks have been subjected to Tertiary regional greenschist facies metamorphism culminating with a temperature of about 450 °C and a pressure between 4 and 6 kbar (Sartori 1990).

Paragenesis and physical properties of turtmannite

Turtmannite occurs as a bright yellow micaceous mineral aligned within the main S_1 schistosity of jacobsite-rich (>80 vol%) paleokarst fillings. Beside jacobsite, turtmannite is associated with minor amounts of kutnohorite, barite, tephroite, and spessartite. Turtmannite is sometimes enriched in thin veinlets cutting these ores at a high angle to the main schistosity. The turtmannite flakes (Fig. 1) measure up to 200 µm in length. The mineral is transparent, with colorless streak and vitreous luster, and it does not show UV or cathodoluminescence. The mineral has a perfect cleavage along {0001}; it is very brittle, and no attempt was made to measure the Vicker's micro-hardness. The calculated density is 3.80(4) g/cm³, for the composition range obtained by the EMP and a cell volume of 12040 Å³. The density was measured by immersing a turtmannite grain in a tube with a density gradient (Clerici solution: Tl formate/Tl malonate/

water system). The solution at the level at which the crystal settled was sampled using a fine chromatography syringe, and the density was deduced from the refractive index. A large range of values was determined ($3.60 < \rho < 4.0$ g/cm³). Air bubbles trapped between open cleavage planes may explain the low values, whereas the highest value was obtained on gemmy crystals that contained tiny inclusions of a black mineral.

Optically, turtmannite is uniaxial negative. The mean refractive index calculated using the Gladstone-Dale relationship and Mandarino's (1976) constants for the range of compositions obtained by EMP is 1.80(2). The measured value of n_o was 1.787(3) (λ = 589 nm, T = 23 °C), by immersion in diiodomethane-sulfur. The refractive index of the immersion liquid was confirmed with a Leitz-Jelley micro-refractometer. No precise measurement could be made for n_e, because of the irregular crystal edges.

Electron microprobe analyses of two different specimens show a relatively large chemical inhomogeneity, both within each sample and between them (Table 1, Fig. 2). This chemical variability is linked to the coupled substitutions Mn = Mg (Fig. 2a) and V = As (Fig. 2b). A mcgovernite-like mineral described from the Kombat mine by Dunn et al. (1988) plots along the same chemical trend as turtmannite (Fig. 2).
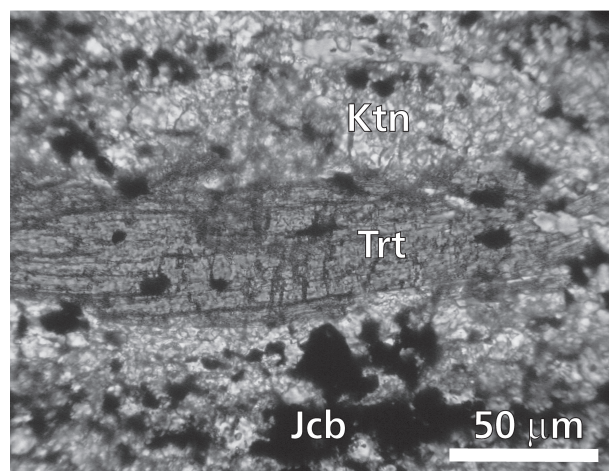
FIGURE 2. Chemical variability of turtmannite from electron microprobe analyses normalized on 29.5 cations, compared to the mcgovernite-like mineral of Dunn et al. (1988). The regression lines were calculated without the mcgovernite-like mineral. (a) Mn vs. Mg (pfu) diagram; (b) As vs. V diagram.

FIGURE 1. Transmitted light microphotograph of a turtmannite aggregate. Jcb = jacobsite, Ktn = kutnohorite, Trt = turtmannite.

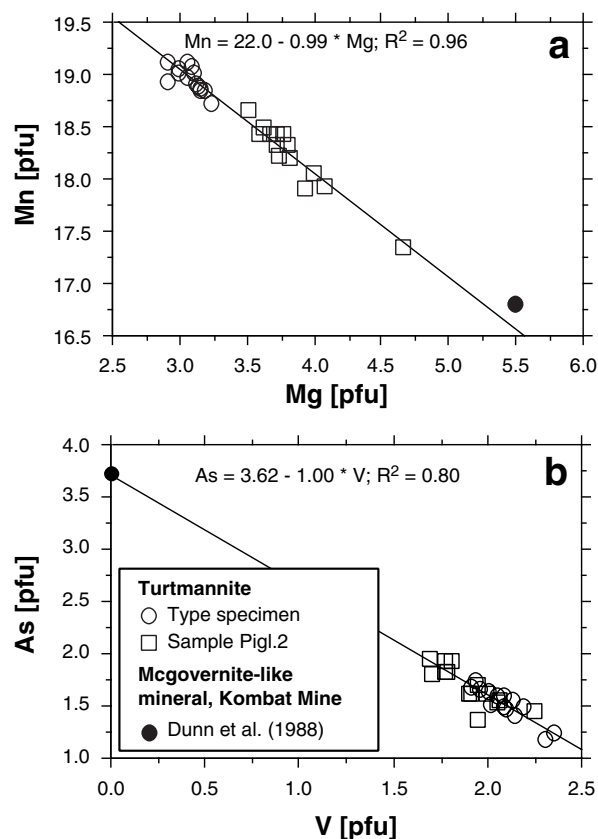**TABLE 1.** Chemical analyses of turtmannite, the mcgovernite-like mineral, and mcgovernite

Oxides	Turtmannite* type material (14 points)			Turtmannite* pigl. 2 (14 points)			Mcgovernite-like†	Mcgovernite‡	Mcgovernite§ average	Mcgovernite‖
	Average	Min.	Max.	Average	Min.	Max.				
V_2O_5	8.09	7.37	9.17	7.42	6.51	8.75				
As_2O_5	7.47	5.82	8.49	8.42	6.96	9.64	13.5	12.48	12.5	13.15
As_2O_3							5.0	4.45	4.6	4.78
SiO_2	8.61	8.48	8.86	8.62	8.25	9.65	9.0	8.92	9.2	8.83
CaO	0.08	<0.05	0.21	0.13	0.05	0.23	0.0	0.0		
MgO	5.27	4.94	5.53	6.63	5.96	8.09	10.2	11.27	11.5	11.02
MnO	57.29	56.58	58.29	55.62	53.01	56.88	53.4	42.72	42.2	42.5
BaO	0.05	<0.05	0.19	0.06	<0.05	0.25				
FeO	<0.05			<0.05				1.53		1.49
CoO	0.13	0.06	0.25	0.05	<0.05	0.13				
NiO	0.21	0.11	0.37	0.26	0.18	0.38				
ZnO	0.06	<0.04	0.13	0.09	<0.05	0.23	0.0	10.22	9.3	10.58
Fe_2O_3							0.3		1.7	
Al_2O_3	0.69	0.60	0.78	0.66	0.51	0.79	1.0		0.0	0.12
H_2O_{calc}	8.06	7.98	8.13	8.13	7.99	8.27	8.49	8.49	9.1	8.30
Total	96.05	95.40	96.97	96.13	94.80	97.63	100.89	100.08	100.1	100.76
Formula based on 29.5 cations, 20.5 H, Z = 12 (occupational variant 2)										
V	2.09	1.91	2.35	1.90	1.69	2.25				
As^{5+}							2.57	2.41	2.42	2.53
As^{3+}							1.11	0.99	1.04	1.07
Σ As	1.53	1.18	1.75	1.70	1.38	1.96	3.68	3.40	3.46	3.60
Si	3.36	3.30	3.49	3.34	3.21	3.67	3.28	3.29	3.41	3.25
ΣV+As+Si	6.98	6.84	7.17	6.94	6.87	7.13	6.96	6.69	6.87	6.85
Ca	0.03	<0.01	0.09	0.05	0.02	0.10				
Mg	3.07	2.98	3.31	3.83	3.50	4.66	5.54	6.20	6.36	6.04
Mn	18.96	18.73	19.13	18.23	17.36	18.66	16.49	13.35	13.25	13.24
Ba	0.01	<0.01	0.03	0.01	<0.01	0.04				
Fe^{2+}								0.47		0.46
Co	0.04	0.02	0.08	0.02	<0.01	0.04				
Ni	0.07	0.04	0.12	0.08	0.06	0.12				
Zn	0.02	<0.01	0.04	<0.03	<0.01	0.07		2.78	2.55	2.87
Fe^{3+}							0.08		0.47	
Al	0.32	0.27	0.36	0.30	0.23	0.36	0.43			0.05
$R_{H/L}$	0.310	0.302	0.321	0.308	0.304	0.319	0.309	0.293	0.304	0.302

Note: Formula normalized to 29.5 cations (variant II). CAMECA SX50 electron microprobe (EMP), operated at 15 kV, 25 nA. Counting time 10 sec. on each peak and 5 sec. on each side of the peak for the background. The beam was defocused to a diameter of about 5 µm. The standards were pure metals for V, Mn, Ni, Co, Cu, Zn; galena for Pb; arsenopyrite for As; wollastonite for Ca and Si; sapphire for Al; strontianite for Sr; benitoite for Ba; rutile for Ti; and hematite for Fe. H_2O is calculated on the basis of 20.5 H pfu.
*,† PbO ≤ 0.13%; TiO_2 ≤ 0.05 wt%; FeO < 0.05 wt%; CuO < 0.03 wt%; SrO ≤ 0.04 wt%.
† Dunn et al. (1988).
‡ Palache and Bauer (1927), Wuensch (1960).
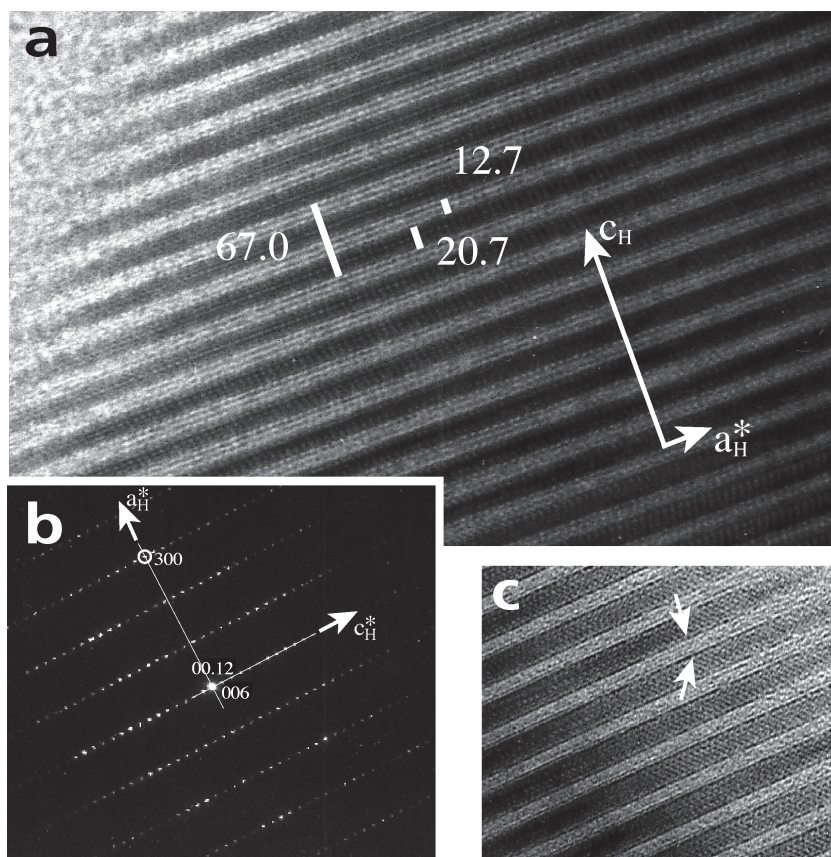§ Dunn and Nelen (1980).
‖ Moore and Araki (1978).

Crystal structure of turtmannite

Preliminary single crystal and transmission electron microscopy study. One yellow, flake-like ($0.080 \times 0.080 \times 0.015$ mm³) single crystal of turtmannite was used for all X-ray investigations. Preliminary Weissenberg and precession photographs indicated that turtmannite is characterized by one very long axis of approximately 70 Å. Such long periodicities cannot be resolved with a standard single-crystal diffractometer operated with Mo$K\alpha$ X-radiation. On the other hand, it was not clear whether the long periodicity was real, or rather an artifact caused either by pseudo-merohedral twinning or by an oriented intergrowth of two phases. For this reason a high-resolution transmission electron microscopic (HRTEM) investigation became necessary to resolve the true periodicity of turtmannite.

The powder obtained by scratching a thin section with veinlets containing the yellow mineral with a steel needle was suspended in acetone. After gentle milling in an agate mortar, a drop of the suspension was deposited on a carbon-coated copper grid. The TEM analysis was performed with a Philips CM 20 instrument operated at 200 keV (point to point resolution 2.9 Å). The selected area electron diffraction pattern confirmed the preliminary monoclinic C-centered unit cell previously determined from X-ray single-crystal photographs: $a_M = 14.29$, $b_M = 8.26$, $c_M = 68.3$ Å, $\beta_M = 94.0°$. Note that it later became evident that the true symmetry of turtmannite was rhombohedral, with $c_H \parallel c_M$ (Fig. 3b). The HRTEM images reveal a perfectly ordered pattern, with a two-layered module defining a 33.5 Å sub-period (Figs. 3a and 3c). The image can be interpreted in two ways: (1) microtwinning or complex polytype, where the difference in contrast between the two modules would be a consequence of a slight misorientation of the sample; (2) a composite structure, containing two chemically and structurally distinct sub-units. Several observations allow us to favor the second hypothesis. (1) A series of pictures was taken after reorienting the sample each time, showing no change in contrast, contrary to what is expected if misorientation was the cause of the contrast. Moreover, the contrast is also visible in the thicker parts of the sample, something that is not expected for misoriented twins or polytypes. (2) The contrast across the layers is symmetrical (arrows in Fig. 3c). (3) The light con-

FIGURE 3. Transmission electron microscopy study of turtmannite. **(a, c)** $[2\bar{1}0]_H$ lattice fringe images of turtmannite taken at different defocus values. In the image **(c)**, the light layers are amorphous due to beam damage whereas lattice fringes are still visible in the dark layers. The contrast on both sides of the layers is similar. **(b)** $[2\bar{1}0]_H$ small area electron diffraction (SAED) pattern of turtmannite. Note that all indices and axes are given in hexagonal setting.

trasted layers are more beam sensitive.

Data collection, structure solution, and refinement. Subsequently to the HRTEM study, a data collection using $MoK\alpha$ X-radiation was attempted with a three-circle SMART system equipped with a CCD detector. Such a diffractometer arrangment has the advantage that the crystal to camera distance is variable allowing for data collection on crystals of high periodicity by choosing a long distance (Burns 1999). Due to the strongly anisotropic shape of the flaky crystal and the heavy elements (mainly Mn) selection of softer X-ray radiation with a longer wavelength (e.g., $CuK\alpha$ as routinely applied to protein crystallography) was not desirable because of anisotropic absorption problems. As a compromise between gain in spatial resolution and loss of diffracted intensity a crystal to camera distance of 12 cm (routine distance is approximately 5.5 cm) and a frame exposure time of 300 s. were chosen for data collection on turtmannite. Nevertheless, strong reflections along c^* contributed significantly to their neighboring c^* reciprocal lattice nodes. The overlap could be minimized by using a smaller rigid box for intensity integration. However, the program SAINT (Siemens 1996a) does not allow this option, and defines the box in terms of the full width at half maximum, and refines the peak shape with a 3D algorithm. Thus it was clear from beginning that the collected data would not be excellent but hopefully sufficient for structure solution. All X-ray reflections were exceptionally sharp without any significant contribution of diffusiveness or streaking. Approximately a half-sphere of reciprocal space was collected comprising 11 196 reflections in agreement with the C-centered monoclinic lattice determined from preliminary Weissenberg and precession photographs. Systematic absences indicated the space groups $C2/c$ or Cc. Neither an empirical nor an analytical absorption correction improved the internal R_{int} value (Table 2) thus the correction was not applied. The structure was solved by direct methods in space group $C2/c$ and was satisfactorily refined using the SHELX-97 program package (Sheldrick 1997). At this stage it became evident that the true symmetry of turtmannite must be rhombohedral thus the monoclinic C-centered cell was transformed by the matrix (0, –1, 0; –0.5, 0.5, 0; –1, 0, –3) yielding a hexagonal cell with $a_H = 8.259(2)$, $c_H = 204.3(3)$ Å, which is very similar to mcgovernite (Wuensch 1960). The corresponding rhombohedral cell has $a_R = 68.31$ Å, $\alpha_R = 6.92°$. Thus in spite of the giant c dimension in the hexagonal setting the periodicity is approximately 68 Å. Subsequent structure refinements using neutral-atom scattering factors were carried out in space group $R\bar{3}c$ (hexagonal setting). All displacement parameters were kept isotropic. If necessary cation occupations were refined using scattering power and bond lengths for appropriate estimates of cation distributions where the chemical composition determined by electron microprobe analyses indicated the most probable assignments. The high R_{int} is caused by the orientation of the crystal and data collection on a three-circle diffractometer. The comparison of identical reflections measured on different frame orientation

TABLE 2. Parameters for X-ray data collection and crystal structure refinement

Diffractometer	Siemens Smart CCD
X-ray radiation	MoKα (0.71073 Å)
X-ray power	55 kV, 40 mA
Temperature	293 K
Crystal size	$80 \times 80 \times 15 \ \mu m^3$
Detector to sample distance	12.0 cm
Rotation axis	φ
Rotation width	0.1°
Total number of frames	3813
Frame size	512×512 pixels
Time per frame	300 s
Space group	$R\bar{3}c$, No. 167
Cell dimensions (Å)	$a = 8.259(2)$, $c = 204.3(3)$
Collection mode	automated hemisphere
Reflection collected	11196
Max. 2θ	50.94
Index range	$-9 \le h \le 7$, $-9 \le k \le 8$, $-242 \le l \le 187$
Unique reflections	2274
Reflections > 4σ(I)	1886
R_{int}	14.91%
R_σ	8.96%
Number of least squares parameters	135
GooF	2.64
$R1$, $I > 4\sigma(I)$	12.36%
$R1$, all data	15.15%
w$R2$ (on F^2)	26.47%

shows that depending on the orientation of the frames in reciprocal space, the tail overlap along **c*** varies. "Rocking curves" obtained with a rigid box (program SMART; Siemens 1996b) for specific reflections suffering from tail overlap did not indicate deviation from rhombohedral symmetry.

X-ray results and structure description

Refined atomic coordinates and site occupancies are given in Table 3. Interatomic distances are summarized in Table 4. The X-ray powder diffraction pattern calculated from the crystal structure model is compared to the measured pattern in Table 5. The relatively poor agreement between calculated and measured intensities is probably related to the chemical and structural complexity of turtmannite, and in particular to varying amounts of the different occupational variants (see below). The oxygen coordination and the bond strength sums (Σ_{bs}) are evaluated in Table 6 using the bond strength concept of Pauling (1929), $\Sigma_{bs} = \Sigma(v/k)$ where "v" is the valence and "k" the coordination number of a cation bonded to a corresponding O atom. This simple type of analysis allows for assignment of OH groups. Due to the disordered character of the structure (discussed below) a bond valence analysis (e.g., Brown 1992) was not performed.

The structure of turtmannite consists of 84 oxygen layers stacked along the **c** axis. The average thickness of a layer is

TABLE 3. Populations, Wyckoff sites (W), atomic positional parameters, and isotropic displacement parameters (U_{iso}) for turtmannite

Atom	Type*	Population	W	x/a	y/b	z/c	U_{iso}
M1	1	0.74(3) Mg + 0.26 Mn	36f	0. 1412(6)	0.4234(6)	0.00010(2)	0.014(2)
M2	2	1 Mn	12c	0	0	0.01010(2)	0.022(1)
T3	2	0.48(3) Mg	36f	0.471(2)	0.100(2)	0.01450(4)	0.006(5)
T4	2	0.89(2) V + 0.11 As	12c	1/3	2/3	0.01440(2)	0.015(2)
M5	3	1 Mn	36f	0.2071(4)	0.2585(4)	0.02374(1)	0.0191(7)
T6	3	0.26(1) As	12c	2/3	1/3	0.02396(5)	0.015(4)
M6	3	0.152(6) Mn	36f	0.897(2)	0.379(2)	0.02351(7)	0.01(fix)
M7	4	0.78(1) Mg + 0.22 Mn	12c	1/3	2/3	0.03491(3)	0.014(3)
M8	4	0.848(6) Mn	36f	0.9039(4)	0.3545(5)	0.03505(1)	0.0173(9)
T9	4	0.51(1) As + 0.49 V	12c	0	0	0.03833(2)	0.013(1)
M10	5	1Mn	36f	0.1189(4)	00.4158(4)	0.04864(1)	0.0158(7)
T11	5	0.76(1) Si + 0.24 As	12c	2/3	1/3	0.04935(3)	0.016(2)
M12	6	1 Mn	12c	0	0	0.04935(3)	0.035(1)
M13	6	1 Mn	36f	0.4217(4)	0.3136(4)	0.06009(1)	0.0153(7)
T14	6	1 Si	12c	1/3	2/3	0.06192(3)	0.012(2)
M15	7	1 Mn	36f	0.1072(4)	0.4013(4)	0.07179(1)	0.0147(7)
T16	7	1 Si	12c	2/3	1/3	0.07321(3)	0.011(2)
T17	8	1 Mn	18e	−0.0746(5)	−0.4079(5)	0.08333	0.0161(9)
T18	8	1 V	12c	0	0	0.08057(2)	0.012(1)
O2	h	1 O	12c	1/3	2/3	0.00573(9)	0.021(5)
O3	h	1 O	36f	0.052(2)	0.799(2)	0.00564(6)	0.028(3)
O4	c	1 O	36f	0.221(2)	0.045(2)	0.01779(6)	0.023(3)
O5	c	1 O	36f	0.385(2)	0.494(2)	0.01705(6)	0.030(3)
O6	c	0.60 O	12c	2/3	1/3	0.0171(2)	0.030(9)
O7	h	1 O	36f	0.6987(2)	0.149(2)	0.02909(6)	0.023(3)
O8	h	1 O	36f	0.561(2)	0.709(2)	0.02922(5)	0.018(3)
O9	h	1 O	12c	0	0	0.02997(8)	0.011(4)
O10	c	1 O	36f	0.959(2)	0.170(2)	0.04116(5)	0.016(2)
O11	c	1 O	36f	0.112(2)	0.607(2)	0.04151(6)	0.022(3)
O12	c	1 O	12c	2/3	1/3	0.04129(8)	0.013(4)
O13	h	1 O	36f	0.637(2)	0.498(2)	0.05276(5)	0.015(2)
O14	h	1 O	36f	0.184(2)	0.233(2)	0.05346(5)	0.015(2)
O15	h	1 O	12c	1/3	2/3	0.05379(9)	0.019(4)
O16	h	1 O	12c	2/3	1/3	0.06513(8)	0.010(4)
O17	h	1 O	36f	0.369(1)	0.505(2)	0.06507(5)	0.010(2)
O18	h	1 O	36f	−0.162(2)	−0.236(2)	0.06573(5)	0.013(2)
O20	n.c.p	1 O	36f	0.872(2)	0.392(2)	0.07631(5)	0.013(2)
O21	n.c.p	1 O	12c	0	0	0.08860(8)	0.015(4)

* n.c.p. = non-close-packed; h = hexagonal close-packing; c = cubic close-packing arrangement.

TABLE 4. Interatomic distances (Å) for turtmannite

M1	O3	1×	2.05(1)		T9	O10	3×	1.70(1)
	O3	1×	2.09(1)			O9	1×	1.71(2)
	O1	1×	2.07(1)		average			1.70
	O1	1×	2.08(1)					
	O1	1×	2.09(1)		M10	O14	1×	2.08(1)
	O2	1×	2.16(1)			O13	1×	2.12(2)
average			2.09			O11	1×	2.17(1)
						O15	1×	2.20(1)
M2	O3	3×	2.12(1)			O10	1×	2.35(1)
	O4	3×	2.29(1)			O11	1×	2.47(1)
average			2.21		average			2.23
T3	O6	1×	1.87(2)		T11	O13	3×	1.65(1)
	O1	1×	1.95(2)			O12	1×	1.65(2)
	O5	1×	1.96(2)		average			1.65
	O4	1×	2.00(2)					
average			1.94		M12	O18	3×	2.13(1)
						O14	3×	2.16(1)
T4	O5	3×	1.76(2)		average			2.15
	O2	1×	1.77(2)					
average			1.76		M13	O17	1×	2.10(1)
						O18	1×	2.13(1)
M5	O8	1×	2.11(1)			O14	1×	2.20(1)
	O7	1×	2.16(1)			O16	1×	2.20(1)
	O4	1×	2.19(1)			O13	1×	2.24(1)
	O4	1×	2.20(1)			O13	1×	2.39(1)
	O5	1×	2.22(1)		average			2.21
	O9	1×	2.33(2)					
average			2.20		T14	O17	3×	1.63(1)
						O15	1×	1.66(1)
T6	O7	3×	1.97(1)		average			1.64
average			1.97					
					M15	O20	1×	2.12(1)
M6	O7	1×	1.99(2)			O18	1×	2.17(1)
	O7	1×	2.12(2)			O19	1×	2.19(1)
	O6	1×	2.18(3)			O17	1×	2.25(1)
	O8	1×	2.20(2)			O17	1×	2.33(1)
	O5	1×	2.28(2)			O21	1×	2.42(1)
	O4	1×	2.28(2)		average			2.25
average			2.18					
					T16	O20	3×	1.64(1)
M7	O8	3×	2.09(1)			O16	1×	1.65(2)
	O11	3×	2.12(1)		average			1.64
average			2.10					
					T17	O20	2×	2.06(1)
M8	O7	1×	2.09(1)			O19	2×	2.12(1)
	O8	1×	2.13(1)		average			2.09
	O10	1×	2.18(1)					
	O7	1×	2.23(1)		T18	O21	1×	1.64(2)
	O12	1×	2.27(1)			O19	3×	1.67(1)
	O11	1×	2.33(1)		average			1.66
average			2.21					

2.43 Å. Twelve close-packed oxygen layers (*c* or *h*) are followed by two non-close-packed (*n*) layers (Table 7). This stacking may be written as …1*h*2*c*3*h*4*c*5*h*6*h*7*n*8*n*7*h*6*h*5*c*4*h*3*c*2*h*… and is repeated six times. In this nomenclature "*h*" means that the oxygen layers above and below have the same stacking order (ABA). "*c*" means that the oxygen layers above and below have a different stacking order (ABC), and "*n*" means that one of the following oxygen layers is not stacked according to close packing. Numbers between the letters indicate the type of cation layers connecting the adjacent oxygen sheets; these are counted serially starting from the $z = 0$ level. Thus, in spite of the large hexagonal *c* parameter the structure consists of only eight symmetrically distinct cation layers (Fig. 4, Table 7). Average interlayer distances are given in Table 8 and indicate that the non-close-packed interlayer (no. 8) is only slightly widened (2.52 Å) compared to the close-packed interlayers. Long interlayer distances (>2.4 Å) in the close-packed sequences are mainly caused by octahedral Mn^{2+} with an ionic radius of 0.82 Å (Shannon 1976). The first layer, which is mainly occupied by Mg octahedra, is only <2.2 Å thick.

Considering the formula $Mn_{234.07}Mg_{53.19}V_{28.55}As_{13.41}$ $Si_{33.12}(O,OH)_{583.2}$, Z = 1, refined from single-crystal X-ray data, the octahedral sites are occupied by 35.93 per formula unit (pfu) Mg and 216.07 pfu Mn. The remaining Mg and Mn atoms, 17.26 and 18 pfu, respectively, occupy tetrahedral sites T3 and T17. The other tetrahedral sites are filled with Si, V, and As. Arsenic occurs in two oxidation states, As^{3+} and As^{5+}, forming either a trigonal pyramid $(As^{3+}O_3)^{3-}$ or a tetragonal $(As^{5+}O_4)^{3-}$ group. The $As^{3+}O_3$ pyramid is only partly occupied. If As^{3+} resides on T6 the oxygen site O6 is vacant to allow the As^{3+} lone electron pair to extend into the vacant position.

Five of the eight cation layers have an ordered arrangement of tetrahedra and octahedra whereas three layers show occupational disorder. Changes of the occupational patterns in layer no. 3 require for electrostatic reasons also changes of the cation distributions in the two adjacent cation layers (no. 2 and 4). In

TABLE 5. Comparison of an experimental powder diffraction pattern with that calculated from the structural model

d obs.*	I vis.*	h	k	l	d calc†	I calc†
		0	0	6	34	100
		1	0	8	6.9	3
		0	0	36	5.7	4
		0	1	22	5.7	3
		1	1	16	6.2	4
5.11	10	1	1	28	5.11	4
		1	0	38	4.30	4
		1	1	0	4.12	10
		2	1	21	3.80	4
		2	1	27	3.62	3
		1	0	50	3.55	4
		0	1	52	3.44	3
		1	2	33	3.43	16
		1	1	36	3.34	3
		1	0	56	3.25	9
		1	1	39	3.24	13
		2	2	28	3.21	2
		0	1	58	3.16	3
		2	1	42	3.15	16
		2	0	34	3.07	4
		2	1	45	3.05	14
2.99	40	0	1	62	2.99	3
		0	2	38	2.98	5
2.93	20	0	2	40	2.93	17
		1	0	64	2.91	3
2.88	20	2	1	51	2.87	20
2.83	40	2	2	44	2.83	36
2.78	20	2	2	46	2.78	7
		1	0	68	2.77	2
2.69	80	3	1	1	2.70	3
		3	2	2	2.70	4
		3	1	7	2.69	19
		3	2	10	2.68	3
		3	1	14	2.66	5
2.64	20	3	2	17	2.63	6
		3	2	19	2.62	2
		3	2	26	2.55	2
		2	1	63	2.55	2
		3	2	28	2.53	3
2.43	60	0	0	84	2.43	3
		1	3	37	2.43	9
		3	2	38	2.41	12
2.38	80	1	2	40	2.39	18
		0	3	0	2.38	8
		3	1	41	2.37	15
		1	2	43	2.35	3
		2	1	44	2.33	2
		2	1	47	2.29	4
		0	0	90	2.27	3
		3	1	53	2.21	3
		2	1	78	2.21	2
		3	0	42	2.14	5
		2	3	59	2.13	2
		2	1	65	2.05	4
		1	2	67	2.02	4
		3	0	54	2.02	2
		2	1	68	2.01	2
1.943	10	1	2	73	1.943	2
1.895	10	3	2	77	1.893	8
		1	3	37	1.865	4
		1	2	82	1.831	3
		1	2	83	1.819	5
1.561	100	1	4	0	1.559	10

* Gandolfi Camera 114.6mm, Cu$K\alpha$ X-radiation; 45 hours exposure.
† Calculated for site occupancies listed in Table 3.

the following discussion the layers will be characterized by the number of occupied octahedral (**M**) and tetrahedral (**T**) positions. For a layer in which only octahedra are occupied the maximum occupancy is seven, thus this layer would be named **M$_7$**. In this nomenclature tetrahedrally coordinated As^{5+} (or Si, V, Mg, Mn) and threefold coordinated As^{3+} (pyramidal AsO$_3$) are not

distinguished and both were designated as **T**. Seven different cation layer types; **M$_3$**, **M$_6$**, **MT**, **M$_3$T**, **M$_4$T**, **MT$_4$**, and **T$_5$** occur in turtmannite including all three occupational variants.

Cation layer no. 1 is composed of 6 octahedra (M1), and is therefore labeled **M$_6$**. The occupancy of M1 octahedra is dominated by Mg with minor Mn^{2+}. The population refinements combined with crystal chemical arguments indicate that for the layers no. 2, 3, and 4 there are three different occupational patterns (I, II, and III), occupied to approximately 50, 33, and 16%, respectively. These three occupational variants will be discussed separately below.

Layer no. 5 (**M$_3$T**) consists of M10 (Mn) triplets and T11 (Si + As). In layer no. 6 (**M$_4$T**) the octahedra M12 and M13 are occupied by Mn atoms and the trifoliate interstices are centered by T14 (Si). Layer no. 7 (**M$_3$T**) consists of M15 (Mn) triplets connected by T16 (Si); therefore layers no. 5 and 7 are very similar. Special attention is paid to layer no. 8 (**T$_5$**) situated between the two non-close-packed oxygen layers. In a close-packed oxygen arrangement tetrahedral voids have the triangular basis parallel to the oxygen sheets. This is not the case for the Mn^{2+}-filled T17 tetrahedra in layer no. 8, situated on twofold axes running perpendicular to the **c** axis. This unusual layer is completed by T18 tetrahedra, filled with V^{5+}, connecting the Mn^{2+} tetrahedra. Although unusual in silicates, Mn^{2+} in tetrahedral coordination is known from numerous close-packed compounds, e.g., synthetic (Fe,Mn)$_2$TiO$_4$ spinel (Sedler et al. 1994). The mean tetrahedral Mn-O distance of 2.09 Å (Table 4) is in the normal and expected range.

Occupational variant I (50%). Layer no. 2 is composed of M2 (Mn), T4 (89% V and 11% As), and a tetrahedron-triplet, T3 (Mg). The layer composition is **MT$_4$**. Layer no. 3 has **M$_3$** composition formed by triplets of Mn-bearing M5 octahedra. Layer no. 4, **M$_4$T**, is composed of M8 (Mn), T9 (51% As and 49% V), and a triplet of M7 (Mg, Mn). The low cation density in layer no. 3 enables higher cation densities in the adjacent layers leading to this sequence along the **c** axis: **MT$_4$** (no. 2) – **M$_3$** (no. 3) – **M$_4$T** (no. 4). This arrangement yields the hypothetical end-member formula for turtmannite of [IV]Mn$_{1.5}$[IV]Mg$_3$[VI](Mn,Mg)$_{21}$[(V,As)O$_4$]$_3$[SiO$_4$]$_3$O$_5$(OH)$_{20}$, Z= 12. In Table 6 the assignment of OH and O atoms to the various oxygen positions is shown.

Occupational variant II (33%). Layer no. 2 is composed of M2 (Mn), T4 (V + As), but T3 is not occupied, yielding an **MT** layer. Layer no. 3 (**M$_3$T**) has in addition to the M5 (Mn) triplets a trigonal pyramidal (As^{3+}O$_3$) group, T6. The O6 position is vacant because of the necessity to accommodate the lone electron pair associated with the (AsO$_3$)$^{3-}$ trigonal pyramid. Among the distances listed in Table 4 only the three T6-O7 bonds of 1.97 Å seem too long for a trigonal As^{3+}O$_3$ pyramid. Expected values are approximately 1.75 Å. This discrepancy is not surprising because the As^{3+}O$_3$ pyramid occurs in the occupational disordered modules and O7 bonds also to the partly occupied sites M6 and M8. Layer no. 4 (**M$_4$T**) is identical to the corresponding sheets in the occupational variant I. The hypothetical formula for turtmannite with the sequence **MT** (no. 2) – **M$_3$T** (no. 3) – **M$_4$T** (no.4) is [IV]Mn$_{1.5}$[VI](Mn,Mg)$_{21}$ [(V,As)O$_4$]$_3$[SiO$_4$]$_3$[AsO$_3$](OH)$_{21}$, Z=12. The assignment of OH molecules is shown in Table 6.
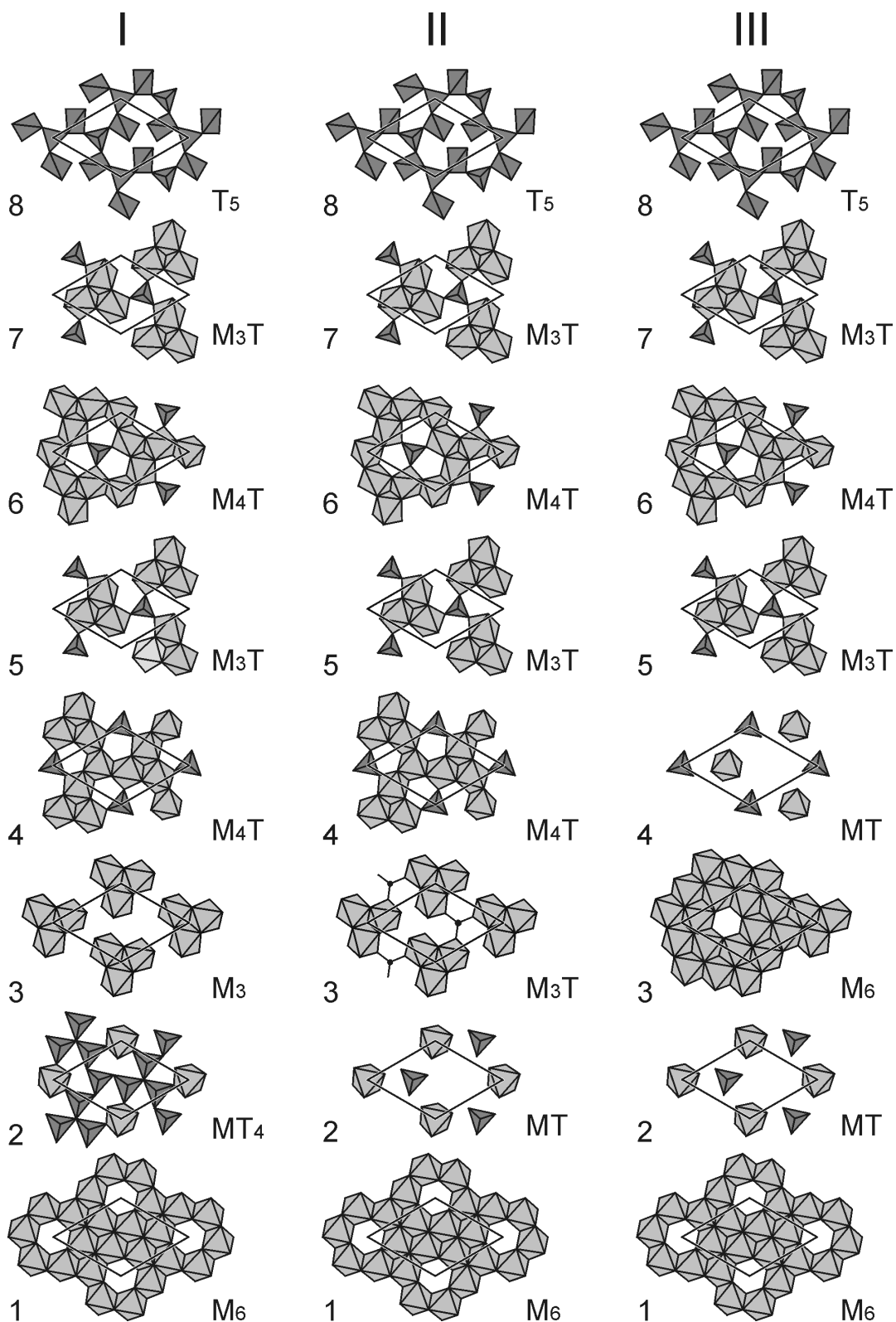
FIGURE 4. The eight different cationic layers in turtmannite, and the three varieties arising from disorder in the layer 3, which causes correlated disorder in the layers 2 and 4. The composition of the layers and the stacking order are summarized in Table 7.

TABLE 6. Bond strength sums (Σ_{bs}) for oxygen atoms in turtmannite allowing for OH assignment

Atom pfu	Cation coordination	Variant 1		Variant 2		Variant 3	
		Σ_{bs}	Species	Σ_{bs}	Species	Σ_{bs}	Species
O1 3×	3× M1 + T3	1.5	O	1	OH	1	OH
O2 1×	3× M1 + T4	2.25	O	2.25	O	2.25	O
O3 3×	2× M1 + M2	1	OH	1	OH	1	OH
O4 3×	M2 + T3 + 2× M5 + M6	1.5	O, OH	1	OH	1.33	O, OH
O5 3×	T3 + T4 + M5 + M6	2.08	O	1.58	O	1.91	O
O6 1×	3× T3 + T6 + 3× M6	1.5	O	–		1	OH
O7 3×	M5 + T6 + 2× M6 + 2× M8	1	OH	2	O	1	OH
O8 3×	M5 + M7 + M8 + M6	1	OH	1	OH	1.33	OH
O9 1×	3× M5 + T9	2.25	O	2.25	O	2.25	O
O10 3×	T9 + M8 + M10	1.91	O	1.91	O	1.58	O
O11 3×	M7 + M8 + 2× M10	1.33	OH	1.33	OH	1	OH
O12 1×	3× M8 + T11	2	O	2	O	1	OH
O13 3×	M10 + T11 + 2× M13	2	O	2	O	2	O
O14 3×	M10 + M12 + M13	1	OH	1	OH	1	OH
O15 1×	3× M10 + T14	2	O	2	O	2	O
O16 1×	3× M13 + T16	2	O	2	O	2	O
O17 3×	T14 + M13 + 2× M15	2	O	2	O	2	O
O18 3×	M12 + M13 + M15	1	OH	1	OH	1	OH
O19 3×	M15 + T17 + T18	2.08	O	2.08	O	2.08	O
O20 3×	T16 + M15 + T17	1.83	O	1.83	O	1.83	O
O21 1×	3× M15 + T18	2.25	O	2.25	O	2.25	O

Note: For variant I it was not clear whether OH should be assigned to O1 or O4 (both have Σ_{bs} = 1.5). OH was assigned to O4 because M-O distances are rather long, indicating slight overbonding. For variant III it was not clear whether OH should be assigned to O4 or to O8 (both with Σ_{bs} = 1.33). OH was for the same reason as for variant I assigned to O4.

TABLE 7. Schematic cation and oxygen packing sequence in turtmannite (nomenclature explained in the text)

Oxygen layer code*	Atom name	Cation layer no.	Layer	$M^{[6]}$ composition	$T^{[4]}$
h	O1, O2, O3	1	M_6	Mn/Mg1	
c	O4, O5, O6	2	MT_4 /MT / MT	Mn2	Mg3, As/V4
h	O7, O8, O9	3	M_3 / M_3T / M_6	Mn5, Mn6	As6
c	O10, O11, O12	4	M_4T / M_4T/ MT	Mn/Mg7, Mn8	As9
h	O13, O14, O15	5	M_3T	Mn10	As/Si11
h	O16, O17, O18	6	M_4T	Mn12, Mn13	Si14
n. c. p.	O19, O20, O21	7	M_3T	Mn15	Si16
n. c. p.	O19, O20, O21	8	T_5		Mn17, V18
h	O16, O17, O18	7	M_3T	Mn15	Si16
h	O13, O14, O15	6	M_4T	Mn12, Mn13	Si14
c	O10, O11, O12	5	M_3T	Mn10	As/Si11
h	O7, O8, O9	4	M_4T / M_4T/ MT	Mn/Mg7, Mn8	As9
c	O4, O5, O6	3	M_3 / M_3T / M_6	Mn5, Mn6	As6 (pyramid)
h	O1, O2, O3	2	MT_4 /MT / MT	Mn2	Mg3, As/V4
		1	M_6	Mg/Mn1	

* n.c.p. = non-close-packed; h = hexagonal close-packing; c = cubic close-packing arrangement.

Occupational Variant III (16%). Layer no. 2 (**MT**) is identical to the occupational variant II (M2, T4). Layer no. 3 (**M6**) has in addition to M5 (Mn) another Mn-bearing octahedral site, M6. In layer no. 4 (**MT**) only M8 (Mn) and T9 (As + V) are occupied whereas the octahedral M7 position is vacant. The high cation density in layer no. 3 requires low cation densities in the adjacent layers to avoid short cation-cation contacts. The sequence **MT** (no. 2) – **M₆** (no. 3) – **MT** (no. 4) leads to the hypothetical end-member formula $^{[IV]}Mn_{1.5}{}^{[VI]}(Mn,Mg)_{21}[(V,As)O_4]_3[SiO_4]_2[SiO_3OH](OH)_{25}$ which is the most hydroxylated variant (Table 6).

DISCUSSION OF HRTEM RESULTS

The HRTEM images, taken close to the Scherzer defocus value, reveal two types of broad bands along the **c** axis (Fig. 3a,c); light bands approximately 12.7 Å wide, composed of

three bright fringes intercalated with two dark fringes, and dark bands approximately 20.7 Å wide, composed of 4 bright and 5 dark fringes. Both bands are periodically repeated along the **c** axis. Both bands are unstable under prolonged exposure to the electron beam, but fringe contrast vanishes more rapidly in the light bands than in the dark bands. The contrast variation is larger among the fringes within the light bands than within the dark bands. A brighter fringe appears within the dark bands on the images recorded at defocus values less than Scherzer defocus. The distance of 12.7 + 20.7 = 33.4 Å corresponds to the 14 layer periodicity that is repeated six times to coincide with the hexagonal *c* parameter of 204 Å. This means that the light 12.7 Å and dark 20.7 Å bands correspond to five and nine cation layers, respectively. For symmetry reasons there are only two possibilities for the alternation of these two types of bands: (1) The light fringe (12.7 Å) represents the cation layer sequence 6-7-8-7-6 and the dark fringe (20.7 Å) represents the nine-layers sequence 5-4-3-2-1-2-3-4-5. (2) The light fringe represents the cation layer sequence 3-2-1-2-3 and the dark fringe represents the nine-layers sequence 4-5-6-7-8-7-6-5-4. The difference in beam sensitivity observed between the two bands is more compatible with interpretation 2. Layers 1 through 3 have, assuming the two most frequent occupational variants 1 and 2, (1) larger underbonding of the O atoms and more hydroxyl groups and (2) lower average electron density than the remaining layers. The extent and the rapidity of beam damage are known to be proportional to the hydroxyl content and are inversely proportional to the average

atomic weight of a structure (Veblen and Buseck 1983). Both factors are compatible with the assignment of the light band to the sequence 3-2-1-2-3. Contrast details such as the brighter fringe in the middle of the dark band are ambiguous and may be explained by both interpretations. The center layer of the 20.7 Å band is layer 1 for interpretation 1 and layer 8 for interpretation 2. Both layers are unique relative to the others with a very small layer thickness and only octahedra occupied for layer 1, and slightly larger than average thickness and only tetrahedra occupied for layer 8. The contrast variation in the bright band may be caused by variations in the occupancies in the cation layers, but may also be caused by beam damage.

In conclusion, we believe that interpretation 2 is correct and each of the white lines contributing to the light 12.7 Å fringes represents a cation sheet without occupied tetrahedral sites. Imaging with higher resolution, contrast simulation, and Electron Energy Loss Spectroscopy investigations are planned to resolve the ambiguous assignment of the bands and to study the spatial distribution of the three occupational variants in turtmannite.

THE STRUCTURE OF TURTMANNITE COMPARED TO RELATED MINERALS

Turtmannite and mcgovernite (Palache and Bauer 1927; Wuensch 1968) have similar lattice constants (Table 9). In addition, the proposed space group $R\bar{3}c$ for mcgovernite conforms with turtmannite emphasizing a close structural relationship between the two minerals. Mcgovernite is only known from

TABLE 8. Cation layer thickness (calculated from the distance between adjacent oxygen layers) and electrons per cation layer

O layer*	Mean z/c of O atoms within a layer	Cation layer	Layer thickness (Å)	Electrons in variant 1	Electrons in variant 2	Electrons in variant 3
		1	2.195	92	92	92
h	0.00537					
		2	2.452	71	45	45
c	0.01737					
		3	2.432	75	108	150
h	0.02927					
		4	2.464	118	118	43
c	0.04133					
		5	2.428	94	94	94
h	0.05321					
		6	2.483	114	114	114
h	0.06536					
		7	2.411	89	89	89
n	0.07867					
		8	2.524	121	121	121
n	0.08930					

* n.c.p. = non-close-packed; h = hexagonal close-packing; c = cubic close-packing arrangement.

TABLE 9. Lattice parameter, space groups, and composition of minerals related to turtmannite (*n* = number of layers with approximate thickness of 2.42–2.43 Å)

Mineral	*a* (Å)	*b* (Å)	*c* (Å)	β (°)	*n*	S.G.	Composition	Structure	Reference
mcgovernite	8.22		205.5		84	Rc	Mn, Mg, Zn, As, Si	–	Wuensch (1960)
turtmannite	8.259		204.3		84	Rc	Mn, V, Si, As, Mg	3	this study
mcgovernite-like	8.224		204.		84	Rc	Mn, Mg, As, Si	–	Dunn et al. (1988)
Fe³⁺ equiv. hematolite	8.28		72.69		30	hex.	Mn, Mg, Fe, As, Zn	–	Dunn and Peacor (1983)
kraisslite	8.22		43.88		18	$P6_322$	Mn, As, Si, Zn, Mg, Fe	–	Moore and Ito (1978)
dixenite	8.233		37.499		15	$R3$	Mn, As, Si, Cu, Fe	3	Araki and Moore (1981)
hematolite	8.275		36.60		15	$R3$	Mn, As, Mg, Al	3	Moore and Araki (1978)
arakiite	14.236	8.206	24.225	93.52	10	Cc	Mn, As, Mg, Zn, Fe, Al	3	Cooper and Hawthorne(1999)
franciscanite	8.152		4.809		2	$P3$	Mn, Si, V	3	Pertlik (1986)
welinite	8.155		4.785		2	$P6_3$	Mn, W, Si, Mg	3	Moore (1969)
örebroite	8.183		4.756		2	$P3$	Mn, Sb, Si, Fe	–	Dunn et al. (1986)

the zinc mine at Sterling Hill, New Jersey. Chemical analyses (Table 9) given for mcgovernite by Palache and Bauer (1927) match well with those of Dunn and Nelen (1980) and Moore and Araki (1978). Thus mcgovernite is a Mn-, Mg-, and Zn-bearing arsenosilicate. A mcgovernite-like mineral (Dunn et al. 1988) from the Kombat mine, Namibia, also with comparable lattice constants and symmetry, is a Mn-Mg-bearing arsenosilicate but without Zn. As is the case with the mcgovernite-like mineral (Dunn et al. 1988), turtmannite has no significant Zn. A further difference of turtmannite to both mcgovernite and the mcgovernite-like mineral is the dominance of VO_4 groups in turtmannite substituting for AsO_4. Thus, turtmannite is a mixed vanadate-arsenate-silicate with Mn^{2+} and Mg.

Neither the structure of mcgovernite nor of the mcgovernite-like mineral have been solved. As demonstrated by Wuensch (1960) the extraordinarily long **c** axis of mcgovernite (204 Å in the hexagonal setting) is not caused by twinning or stacking polytypism. The same is true for turtmannite. Wuensch (1968) noticed the similarities in the lattice constants and diffraction symmetries of mcgovernite, hematolite, and dixenite and proposed a layer-like arrangement for these related structures. The structure of hematolite, $(Mn^{2+},Mg,Al)_{15}(OH)_{23}(AsO_3)(AsO_4)_2$, $a = 8.275$, $c = 36.60$ Å, space group $R3$, was subsequently solved (Moore and Araki 1978) and described to be composed of close-packed oxygen layers. Arakiite, $(Mn^{2+}, Mg,Zn, Fe^{3+}, Al)_{15}$ $(OH)_{23}(AsO_3)(AsO_4)_2$, $a = 14.236$, $b = 8.206$, $c = 24.225$ Å, $\beta = 93.52°$, space group Cc, is closely related to hematolite (Cooper and Hawthorne 1999). In hematolite five topologically distinct cation layers can be distinguished. One of these cation layers of M_4T composition is identical to the one found in the minerals welinite (Moore 1967), franciscanite (Pertlik 1986), örebroite (Dunn et al. 1986), and in synthetic $(Mg_2SiO_4)_2[(Mg(OH)_2]_3$ (Horiuchi et al. 1979). Moore and Araki (1978) proposed that the five hematolite cation layers are basic units that also make up the structures of related dixenite, mcgovernite, and kraisslite, and they presented structural models for the structures of dixenite and mcgovernite. For dixenite (Araki and Moore 1981) the proposal was found to be only partly correct. Only some of the hematolite-type layers could be found in dixenite, but the presence of an unexpected Cu-As-cluster and a new layer-type were not foreseen.

Assuming an approximate layer thickness of 2.42–2.43 Å, the c-axis length gives information on the repeat sequence of the respective structure. With $c = 204$ Å (hexagonal setting) mcgovernite, the mcgovernite-like mineral, and turtmannite have a 84-layer repeat structure in common. If we assume that turtmannite and mcgovernite possess identical or at least very similar sequences of cation layers the structural model for mcgovernite (Moore and Araki 1978) must be partly revised. Their most important prediction, however, that a continuous close-packing of O atoms is not preserved in mcgovernite is probably correct, considering the topology of cation layer no. 8 in turtmannite. The interface between the two non-close-packed oxygen layers is formed by a cation sheet T_5 with the exact arrangement and symmetry predicted by Moore and Araki (1978). Their drawing of the predicted Zn_3Si_2 (T_5) layer in mcgovernite is topologically identical to the $Mn_3^{2+}V_2^{5+}$ layer found in turtmannite. Two non-close-packed oxygen layers within a series of close packed layers (*..nnhch..)* have also been observed

in arakiite (Cooper and Hawthorne 1999). The second prediction that a complete sequence of the five-layer module known from hematolite is preserved in turtmannite or mcgovernite could not be confirmed. This can easily be seen because hematolite has an oxygen stacking sequence *..hhhch…* whereas in turtmannite the sequence is *…hchchhnnhhchch...* In other words, four adjacent "*h*" oxygen layers do not occur in turtmannite, which is the reason for the modified cation stacking sequence. Nevertheless, the sequence of four cation layers M_6 (no. 1), MT (no. 2), M_3T (no. 3), M_4T (no. 4) observed for the occupational variant 2 shows strong similarity with hematolite where even the AsO_3 pyramid is preserved in the M_3T layer.

The seven different cation layer types (M_3, M_6, MT, M_3T, M_4T, MT_4, and T_5) recognized in all three occupational variants of turtmannite may be considered building blocks or modules of different chemical composition. Some of the layer types occur twice or even three times within the structure of turtmannite, although with variations in chemistry. Similar modules were also found in the structures of related minerals. Hematolite (Araki and Moore 1981) has the layers M_6, MT, M_3T, and M_4T is common with turtmannite, whereas only the layers M_3, MT_4, and T_5 are unique for turtmannite. Structures composed of such modules are often described with the concept of homologue series or polysomatism (Merlino 1997). The total of seven different modules is of course rather high and therefore unusual. It is clear that the huge variety of chemical compositions for each module makes structure predictions very difficult.

The three occupational variants observed in turtmannite allow predictions to be made concerning the cation stacking in mcgovernite (Palache and Bauer 1927; Wuensch 1960) and in the mcgovernite-like mineral described by Dunn et al. (1988). The ratio between tetrahedral high valence cations (As + Si + V), including pyramidal As^{3+}, and the remaining cations is characteristic of the occupational variant in these minerals. This implies that, because of size and charge differences, substitution of Mg, Mn^{2+}, Fe^{2+}, and Zn for As^{5+}, As^{3+}, V^{5+}, and Si^{4+} will be unfavorable. However, the role of Al^{3+} and Fe^{3+}, though occurring only in low concentrations in mcgovernite and the mcgovernite-like mineral, remains unclear. Here Al^{3+} and Fe^{3+} are treated together with Mg, Mn^{2+}, Fe^{2+}, and Zn. Thus, the high valence/low valence cation-ratio, $R_{H/L}$, in turtmannite is 0.235, 0.312, and 0.267 for the occupational variants 1, 2, and 3, respectively. Based on the average analyses for mcgovernite provided by Dunn and Nelen (1980) and the analysis for the mcgovernite-like mineral (Dunn et al. 1988), $R_{H/L}$ becomes 0.304 and 0.309, respectively. This indicates that these two minerals crystallize in the occupational variant 2. This is also confirmed by the analytically determined As^{3+} concentration in mcgovernite (Dunn and Nelen 1980), which leads to 1.1 As^{3+} pfu (theoretically value is 1.0 As^{3+} pfu) if the analyses are normalized to 29.5 cations as derived above for occupational variant 2. The average chemical analyses of turtmannite (Table 1) yield an $R_{H/L}$ of 0.310 indicating that the average turtmannite composition is also best described by the occupational variant 2.

ACKNOWLEDGMENTS

REFERENCES CITED

Araki, T., and Moore, P.B. (1981) Dixenite, $Cu^{1+}Mn^{2+}_{14}Fe^{3+}(OH)_6(As^{3+}O^3)_5$ $(Si^{4+}O_4)_2(As^{5+}O_4)$: metallic $[As_3^+Cu^{1+}]$ clusters in an oxide matrix. American Mineralogist, 66, 1263–1273.

Argand, E. (1911) Les nappes de recouvrement des Alpes pennines et leurs prolongements structuraux. Matériel pour la Carte Géologique Suisse, 31, 1–26.

Brown, I.D. (1992) Chemical and steric constraints in inorganic solids. Acta Crystallographica, B48, 553–572.

Burns, P.C. (1999) A new complex sheet of uranyl polyhedra in the structure of wolsendorfite. American Mineralogist, 84, 10, 1661–1673.

Cooper, M.A. and Hawthorne, F.C. (1999) The effect of differences in coordination on ordering of polyvalent cations in close-packed structures: the crystal structure of arakiite and comparison with hematolite. Canadian Mineralogist, 37, 1471–1482.

Dunn, P.J. and Nelen, J.A. (1980) Kraisslite and mcgovernite: new chemical data. American Mineralogist, 65, 957–960.

Dunn, P.J., Peacor, D.R., Erd, R.C., and Ramik, R.A. (1986) Franciscanite and örebroite, two minerals from California and Sweden, related to redefined welinite. American Mineralogist, 71, 1522–1526.

Dunn, P.J., Francis, C.A., and Innes, J. (1988) A mcgovernite-like mineral and leucophoenicite from the Kombat mine, Namibia. American Mineralogist, 73, 1182–1185.

Escher, A., Masson, H., and Steck, A. (1987) Coupes géologiques des Alpes occidentales suisses. Service Hydrologique et géologique national, Rapports géologiques Numéro 2, 11 pp. (with tables).

Gerlach, H. (1869) Die Penninischen Alpen. Denkschriften der Schweizerischen Naturforschenden Gesellschaft, 23.

Horiuchi, H., Morimoto, N., Yamamoto, K., and Akimoto, S.I. (1979) Crystal structure of $((Mg_2SiO_4)_2)(Mg(OH)_2)_3$, a new high pressure structure type. American Mineralogist, 64, 593–598.

Mandarino, J.A. (1976) The Gladstone-Dale relationship. Part I: derivation of new constants. Canadian Mineralogist, 14, 498–502.

Merlino, S. (Ed.) (1997) Modular aspects of minerals. Eötvös University Press/European Mineralogical Union, Budapest.

Moore, P.B. (1967) The crystal structure of welinite, $(Mn^{+4},W)_{<1}(Mn^{+2},W,Mg)_{<3}$ $Si(O,OH)_7$. Arkiv för mineralogi och geologi, 4, 24, 459–466.

Moore, P.B. and Araki, T. (1978) Hematolite, a complex dense-packed sheet structure. American Mineralogist, 63, 150–159.

Palache, C. and Bauer, L.H. (1927) Mcgovernite, a new mineral from Sterling Hill, New Jersey. American Mineralogist, 12, 373–374.

Pauling, L. (1929) The principles determining the structure of complex ionic crystals. Journal of the American Chemical Society, 51, 1010–1026.

Pertlik, F. (1986) The crystal structure of franciscanite, $Mn_3(V_x\square_{1-x})(SiO_4)(O,OH)_3$, [x = 0.5]. Neues Jahrbuch für Mineralogie, Monathefte, 1986, 493–499.

Sartori (1990) L'unité du Barrhorn. Mémoire de Géologie (Lausanne), 6, 156 p.

Schafer, M. (1994) Die Ni-Co-Vererzungen im Turtmantal, Wallis, Schweiz. Unpublished Ph. D. Thesis University of Basel, Switzerland.

Sedler, I.K., Feenstra, A., and Peters, T. (1994) An X-Ray powder diffraction study of synthetic $(Fe,Mn)_2TiO_4$ Spinel. European Journal of Mineralogy, 6, 873–885.

Shannon, R.D. (1976) Revised effective ionic radii and systematic studies of interatomic distances in halides and chalcogenides. Acta Crystallographica, A32, 751–767.

Sheldrick, G.M. (1997) SHELX-97, program for crystal structure determination. University of Göttingen, Germany.

Siemens (1996a) SAINT, release 4.0. Siemens Energy and Automation Inc., Madison, Wisconsin.

———(1996b) SMART, operating system for SMART 1000. Siemens Energy and Automation Inc., Madison, Wisconsin.

Veblen, D.R. and Buseck, P.R. (1983) Radiation effects on minerals in the electron microscope. Proceedings of the 41st Annual Meeting of the Electron Microscopy Society of America.

Wuensch, B.J. (1960) The crystallography of mcgovernite, a complex arsenosilicate. American Mineralogist, 45, 937–945.

———(1968) Comparison of the crystallography of dixenite, mcgovernite and hematolite. Zeitschrift für Kristallographie, 127, 309–318.